Cite this article
Devi K, Das BS, Khuntia JR and Khatua KK
Analytical solution for depth-averaged velocity and boundary shear in a compound channel.
Proceedings of the Institution of Civil Engineers – Water Management,
https://doi.org/10.1680/jwama.18.00062

Research Article
Paper 1800062
Received 24/07/2018;
Accepted 15/01/2021

Keywords: hydraulics & hydrodynamics/ mathematical modelling/river engineering

Water Management

ice Publishing

Analytical solution for depth-averaged velocity and boundary shear in a compound channel

Kamalini Devi MTech, PhD
Associate Professor, Department of Civil Engineering, Vidya Jyothi Institute of Technology, Hyderabad, India (Orcid:0000-0002-5916-3256) (corresponding author: kamalinidevi1@gmail.com)

Jnana Ranjan Khuntia MTech, PhD
Assistant Professor, Department of Civil Engineering, St. Martin's Engineering College, Secunderabad, India (Orcid:0000-0003-3943-4220)

Bhabani Shankar Das MTech, PhD
Assistant Professor, Department of Civil Engineering, National Institute of Technology Patna, Bihar, India (Orcid:0000-0003-1140-0432)

Kishanjit Kumar Khatua MTech, PhD
Professor, Department of Civil Engineering, National Institute of Technology Rourkela, Odisha, India

Estimation of streamwise depth-averaged velocity and boundary shear stress are important requisites for modelling of river flows associated with flood events. Recently, many methods have emerged to predict these flow variables with great accuracy, but they provide unsatisfactory results in shear layer regions. This paper presents an improved methodology to predict depth-averaged velocity and bed shear stress for a straight compound channel flow. An analytical solution to the depth-integrated turbulent form of the Navier–Stokes equation is obtained. The transverse shear stress in the mixing region is modelled using an effective eddy viscosity concept that contains horizontal coherent structures and three-dimensional bottom turbulence. The secondary flow term is modelled by considering the log-law profile for streamwise velocity and half cosine curve for the transverse velocity component. The analytical solution is successfully applied to a wide range of experimental compound channels and field cases. The efficacy of the present solution has been successfully tested by comparing with observed values.

Notation

A	cross-sectional area
b	semi width of main channel
C_{m}	coefficient of mixing layer
E	Nash–Sutcliffe efficiency
f	Darcy–Weisbach friction factor
$\boldsymbol{g}$	gravitational acceleration
H	main channel flow depth
H_{m}	mean water depth
I_{d}	index of agreement
K	Karman constant universally adopted as a characteristic of turbulence
k	empirical coefficient, also function of geometry and roughness
N	number of samples
n	Manning's roughness constant
O_i	observed values
$O_{i\ \mathrm{mean}}$	mean of the observed values
P_i	predicted values
$\%Q_{\mathrm{mc}}$	percentage of flow in the main channel
R	hydraulic radius
R^2	coefficient of determination
S_0	bed slope in x-direction
s	main channel bank slope
$\tilde{U}$	longitudinal velocity
U_*	shear velocity
U_{d}	depth-averaged longitudinal velocity
U_{d}^2	lateral gradient of squared velocity
u'	fluctuating velocity in x-direction
$\tilde{V}$	transverse velocity component
$V_{\max}$	maximum transverse mean velocity
v'	fluctuating velocity in y-direction
w'	fluctuating velocity in z-direction
y	lateral dimension
z_0	elevation above the bed
α	width ratio
β	relative flow depth
δ	mixing layer width
δ/H	non-dimensional mixing layer width
ϑ_{t1}	eddy viscosities due to bottom friction
ϑ_{t2}	eddy viscosities due to large horizontal coherent structure
λ_1	total eddy viscosity due to bottom turbulence
λ_2	total eddy viscosity due to horizontal coherent structures
$\lambda_{2\mathrm{s}}$	additional coefficients for side slope
ρ	density of water
$\left(\rho\tilde{U}\tilde{V}\right)_{\mathrm{d}}$	depth-averaged secondary flow
$-\rho\overline{u'v'}$	turbulent shear stress
τ_{b}	boundary shear stress
τ_{yx}	transverse turbulent shear stress
ϕ	varying depth of flow

1. Introduction

Rivers consisting of a main channel accompanied by one or two flood plains are termed compound channels. In such channels, the hydrodynamic processes are very complex owing to the variation in geometry and roughness. Estimation of the transverse distribution of velocity is essential in predicting

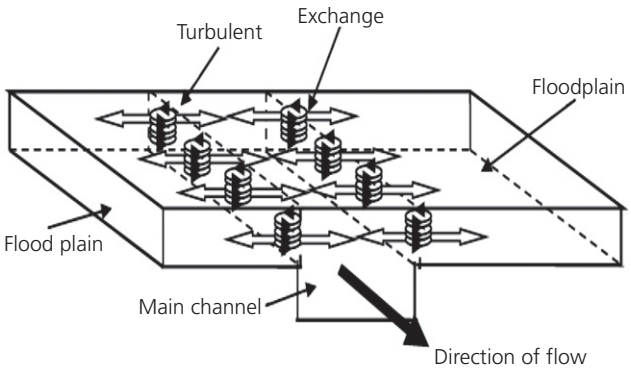

Figure 1. Schematic view of momentum transfers between main channel and flood plain of a two-stage compound channel section (Khatua and Patra 2007)

the stage–discharge relationship and boundary shear stress distribution for overbank flow conditions. A schematic view of a compound channel is presented in Figure 1. It is well known that the faster velocity in the main channel is retarded by the slower moving flood plain, leading to a large transverse exchange of momentum and reduction in overall conveyance capacity. In understanding the behaviour of rivers during the flood, secondary flow effects play an important role in estimating the lateral distribution of velocity and boundary shear stress (Knight *et al*., 2007; Shiono and Knight, 1989). Some complex flow phenomena are also dominated by a blend of bed-generated turbulence and free shear turbulence. So, to account for the additional flow resistance caused by momentum exchange, it is crucial to have a deep understanding of both the secondary flow effect and the turbulence mechanism.

Turbulence structures of a compound channel have been studied by Prinos *et al*. (1985) and Tominaga *et al*. (1989). Turbulence models depending upon some empirical constants have been proposed by Kawahara and Tamai (1988), Krishnappan and Lau (1986) and Larsson (1986). For calibration of these models, direct measurements of the Reynolds shear stresses and secondary flow are essential. Accurate evaluation of the secondary flow structures is essential in estimating the flow parameters, as the strength of these secondary cells greatly affects the anisotropic turbulence generated in the corner region and near the free surface of a compound channel (Knight *et al*., 2007). Van Prooijen *et al*. (2005) separated the half of a compound channel into two uniform zones and one transverse mixing zone. The lateral mass and momentum exchange in each uniform zone is zero because of the same bottom level. However, in the mixing zone, a large amount of mass and momentum transfer occurs between the main channel and flood plains due to the lateral gradients in bed level and longitudinal velocity. For accurate determination of discharge in a river, a proper evaluation of the streamwise velocity in the mixing region needs to be procured. Transverse variation of these streamwise velocities has also been studied by Shiono and Knight (1991), Lambert and Sellin (1996); Ervine *et al*. (2000) and Van Prooijen *et al*. (2005).

The secondary flow phenomena were experimentally investigated by Tominaga and Nezu (1991) and Shiono and Knight (1991). This secondary flow can be estimated by depth integrating the product of vertical variations of streamwise and lateral components of velocities, as the secondary circulations are associated with horizontal flow structures with vertical axes moving in a downstream direction. In low overbank flow cases, the turbulence generated by the bottom friction and transverse shear can be revealed in the form of large horizontal coherent structures with a vertical axis whose length scale is considerably larger than the flow depth (Uijttewaal and Booij, 2000; Van Prooijen *et al*., 2005; Van Prooijen and Uijttewaal, 2002). Evaluation of these mechanisms turns out to be arduous, as is evident from the works of Shiono and Knight (1991), Lambert and Sellin (1996), Ervine *et al*. (2000) and Van Prooijen *et al*. (2005). The applicability of their models with calibration of empirical constants could not be guaranteed for channels of other geometries as they have considered one of the mechanisms as important but neglected others. Most of the works are reported for the estimation of depth-averaged velocity but nothing is mentioned regarding the accurate modelling of the boundary shear stress distribution, especially at the mixing region (Ervine *et al*., 2000; Shiono and Knight, 1991; Van Prooijen *et al*., 2005). Looking at these points of view, the mechanisms accounting for the exchange of momentum and secondary flow are further described and evaluated in the present paper. On the basis of the eddy viscosity concept, a transverse shear stress term is proposed. The secondary flow term is also quantified considering the vertical distribution of streamwise and transverse velocity components. Therefore, the logarithmic distribution of the streamwise velocity component and half-cosine distribution of the transverse velocity component are considered. In this way, the shortfall of the secondary flow effect and momentum transfer of a compound channel is compensated. An analytical solution of the new form of second-order depth-averaged Navier–Stokes equation is presented. The accuracy of the solution is confirmed by the evidence of the results found for both transverse distributions of depth-averaged velocity and boundary shear stress applied to many experimental and natural river data sets.

2. Previous study

To compute the transverse profile of depth-averaged velocity and boundary shear stress in open channel flow, the depth, and time-averaged momentum equation have been solved by various investigators – notably by Shiono and Knight (1991), Ervine *et al*. (2000) and Van Prooijen *et al*. (2005). Their investigations were based on the solution of Reynolds averaged Navier–Stokes equations. For steady and uniform flow, the momentum equation combined with the continuity equation is

expressed as

$$1.\quad \rho\left(\frac{\partial \bar{U}\bar{V}}{\partial y}+\frac{\partial \bar{U}\bar{W}}{\partial z}\right)=\rho \boldsymbol{g}S_0+\frac{\partial}{\partial y}\left(-\rho\overline{u'v'}\right)+\frac{\partial}{\partial z}\left(-\rho\overline{u'w'}\right)$$

where ρ is the water density; S_0 is the bed slope in the x-direction; $\boldsymbol{g}$ is the gravitational acceleration; $\bar{U}$ and u', $\bar{V}$ and v', $\overline{W}$ and w' are the temporal mean velocity components and their corresponding fluctuations in the x-, y- and z-directions. The over bar denotes the time-averaged parameters. Based on the eddy viscosity approach and considering the mean vertical velocity component $(\bar{w})$ as negligible, Shiono and Knight (1991) simplified Equation 1 by integrating it over the flow depth.

$$2.\quad \rho\frac{\partial H\left(\bar{U}\bar{V}\right)_{\mathrm{d}}}{\partial y}=\rho H\boldsymbol{g}S_0+\frac{\partial}{\partial y}\left[\rho\lambda H^2\left(\frac{f}{8}\right)^{1/2}U_{\mathrm{d}}\frac{\partial U_{\mathrm{d}}}{\partial y}\right]-\frac{f}{8}\rho U_{\mathrm{d}}^2\sqrt{1+\frac{1}{s^2}}$$

where H is the flow depth; U_{d} is the depth averaged velocity; λ is the eddy viscosity coefficient; f is the friction factor; and s is the side slope. Shiono and Knight (1991) converted this equation to a second-order linear ordinary differential equation form. They prescribed the boundary condition in each domain of the channel and presented analytical solutions for both constant flow depth domain and variable flow depth domain. The solution was capable of providing depth-averaged velocity and boundary shear stress across the channel. Analysing the flood channel facility experiments, they specified constant values for the gradient of depth-averaged secondary flow $\left(\rho\bar{U}\bar{V}\right)_{\mathrm{d}}$ in the main channel and flood plain. However, the secondary flow contribution in the mixing layer was not considered by Shiono and Knight (1991). According to Tominaga and Nezu (1991) the contribution of secondary flow is found to be maximal at the mixing regions. Knight *et al.* (2007) stated that the boundary shear stress predictions by Shiono and Knight (1991) do not match with the experimental results, owing to improper accounting of the secondary current cell. They therefore improved the boundary shear stress prediction at the bank slope of a simple trapezoidal channel by dividing half of this channel into four panels and specifying constant values for secondary flow and roughness parameters in each panel. For river channels with overbank flow condition, the secondary flow is more significant due to intense three-dimensional (3D) mixing at junctions; so, the flow mechanisms are dominated by the formation of secondary cells together with the effects of horizontal shear and mass transfer. Ervine *et al.* (2000) modelled the secondary flow term $\left(\rho\bar{U}\bar{V}\right)_{\mathrm{d}}$ of the Shiono and Knight method (SKM) by assuming the temporal mean streamwise and transverse velocity components are fractions of depth-averaged velocity. Their model (Equation 3) scales with the gradient of the squared velocity and depends on an empirical coefficient K, which is further a function of geometry and roughness.

$$3.\quad \frac{\partial}{\partial y}\rho HKU_{\mathrm{d}}^2=\rho H\boldsymbol{g}S_0+\frac{\partial}{\partial y}\left[\rho\lambda H^2\left(\frac{f}{8}\right)^{1/2}U_{\mathrm{d}}\frac{\partial U_{\mathrm{d}}}{\partial y}\right]-\frac{f}{8}\rho U_{\mathrm{d}}^2\sqrt{1+\frac{1}{s^2}}$$

Kordi *et al.* (2015) showed that the predicted depth-averaged velocity results found from the model of Ervine *et al.* (2000) are poorer when compared with the SKM, particularly in the interface zone. This is because they assumed a single value of K for all the sub-compartments. However, the magnitude of K should be different from zone to zone to describe the individual 3D mixing process. Again, they modelled the value of K by taking a small number of data sets. Van Prooijen *et al.* (2005) presented a model (Equation 4) for transverse turbulent shear stress (τ_{yx}) in the mixing region of a compound channel. They incorporated the effects of both horizontal coherent structures and 3D bottom turbulence in the transverse turbulent shear stress term.

$$4.\quad \tau_{yx}=\rho\left[\lambda\sqrt{\frac{f}{8}}HU_{\mathrm{d}}\frac{\partial U_{\mathrm{d}}}{\partial y}+\frac{H_{\mathrm{m}}}{H}(\beta\delta')^2\left|\frac{\partial U_{\mathrm{d}}}{\partial y}\right|\frac{\partial U_{\mathrm{d}}}{\partial y}\right]$$

where H is the local water depth; H_{m} is the mean water depth; β is the proportionality constant; and δ is the mixing layer width. Considering that the secondary flow has minor importance on momentum exchange in straight overbank flow cases, this term was neglected when modelling the depth-averaged velocity. However, no information is available for modelling of the bed shear stress. Shiono and Rameshwaran (2015) stated that the model of Van Prooijen *et al.* (2005) over-predicts the bed shear stress considerably in the main channel region. Shiono and Rameshwaran (2015) proposed a model for transverse turbulent shear stress, adopting three mechanisms of momentum exchange in compound channels with emergent vegetation on the flood plain. Their model is expressed as

$$5.\quad \tau_{yx}=\rho\lambda\sqrt{\frac{f}{8}}HU_{\mathrm{d}}\frac{\partial U_{\mathrm{d}}}{\partial y}+\rho\beta\delta U_{\mathrm{d}}\frac{\partial U_{\mathrm{d}}}{\partial y}+\frac{(\rho H\boldsymbol{g}S_0-\tau_{\mathrm{b}})y}{H}$$

The first term on the right-hand side of the equation refers to the momentum exchange due to shear-generated turbulence, the second term refers to the bed-generated turbulence and the third term can be attributed to large horizontal eddy. Applying their model within SKM, they predicted the flow variables of a compound channel with vegetated flood plains. Without the new momentum transfer term (the third term), the SKM over-predicts both the velocity and boundary shear stress in the

main channel and under-predicts them on the flood plain. Following the information from earlier investigations – for example, Tominaga and Nezu (1991) and Rameshwaran and Shiono (2007) – they stated that the secondary flow might not be responsible for the difference between the magnitude of weight component and bed shear stress, occurring outside the shear layer region. However, they found that the third term of their model (momentum exchange due to large horizontal eddy) is simply replaced by the secondary flow concept, as suggested by Shiono and Knight (1991), and suggested inclusion of the appropriate secondary flow term in order to predict the accurate bed shear stress. The applicability of the method is limited to the case of vegetative compound channels in the laboratory only.

3. Present study

Shiono and Knight (1991) evaluated the secondary flow term as the difference between turbulence shear stress and apparent shear stress. The values for secondary flow $\rho(\bar{U}\bar{V})_{\mathrm{d}}$ are plotted along the cross-channel distance of the compound channel and found to be of maximum value in the shear layer regions. Outside the shear layer regions – that is, towards the centre of the main channel and also towards the flood plain wall – the secondary flow effect becomes weaker. This may be due to the infirmity in vertical distribution of transverse velocity in the regions outside the shear layer. Further, the gradient of the secondary flow term is found to be very high in the interface region due to the large difference in velocity between the sub-sections. The gradient becomes lower towards the main channel centre and also towards the flood plain walls. Therefore, secondary flows are more significant in overbank flows and should be included in the governing equation of a flow model (Ervine *et al*., 2000). In this context, a new formulation is proposed for estimating the secondary flow term $\rho(\bar{U}\bar{V})_{\mathrm{d}}$. To quantify the magnitude of $\rho(\bar{U}\bar{V})_{\mathrm{d}}$ in transverse uniform zones, log law can be used to define the streamwise velocity distribution $(\bar{U})$. This has been confirmed from the measured vertical velocity profile in many experimental channels including flood channel facility (FCF) straight compound channels (Knight and Shiono 1990; Wormleaton, 1996; Yang *et al*., 2004). This law states that the dimensionless velocity component – that is, the ratio of temporal mean velocities $(\bar{U})$ to shear velocity (U_*) is linearly proportional to the logarithmic distance normal to the boundary (z). The universally recognised log law can be written as follows:

$$\text{6a.}\quad \frac{\bar{U}}{U_*} = \frac{1}{K}\ln\frac{z}{z_0}$$

where z_0 is the elevation above the bed where the extrapolated logarithmic velocity profile goes through zero and K is the Karman constant universally adopted as a characteristic of turbulence. Yang *et al*. (2004) presented the clear picture about this log law and found the range of the Karman constant variation between 2.43 and 2.5 for open channels. Transverse velocity component $(\bar{V})$ profile of the secondary flow term $\rho(\bar{U}\bar{V})_{\mathrm{d}}$ is inconvenient to determine, as no systematic experimental measured data are available (Van Prooijen *et al*., 2005). The profiles of the temporal mean transverse velocity component $(\bar{V})$ of FCF channels are also not yet published. As stated by Wormleaton (1996), the vertical profile of the transverse velocity component $(\bar{V})$ should satisfy three constraints: (*a*) zero velocity at bed; (*b*) zero shear at water surface; and (*c*) continuity law for steady flow. Following the work of Wormleaton (1996), the vertical profile of the transverse velocity component is graphically presented by Shiono and Knight (1989) and Knight *et al*. (2007). They presented the distributions of shear stress by taking care of secondary flow values in the main channel and flood plain regions. Although Knight *et al*. (2007) presented two measured transverse velocity profiles for simple channel cases, to the present authors' knowledge, the magnitudes of transverse velocity have not been demonstrated in a general sense for a compound channel case.

To obtain the transverse velocity profile of a compound channel, the procedure followed by Van Prooijen *et al*. (2005) has been adopted here. Figure 2 demonstrates the vertical distribution of the streamwise velocity component, transverse velocity component and the product of both distributions. The depth-averaged term $(\bar{U}\bar{V})_{\mathrm{d}}$ of the term $\bar{U}\overline{V}$ is shown by the dashed line in this figure. A simple half cosine approximation is considered for transverse velocity components as

$$\text{6b.}\quad \bar{V} = -V_{\max}\cos\left(\frac{\pi z}{H}\right)$$

where $V_{\max}$ is the maximum transverse mean velocity. Integrating the product of two velocity profiles as written in Equations 6a and 6b over the total flow depth provides the depth-averaged value of secondary flow components. The shear velocity (U_*) is expressed in terms of friction factor (f) and depth-averaged velocity (U_{d}) – that is, $U_* = \sqrt{f/8}U_{\mathrm{d}}$. The term $\sin(\pi z/H)$ is approximated by Taylor series approximation by truncating the series after two terms, as the values after these terms become negligible. The depth-averaged value of $\rho(\bar{U}\bar{V})$ is now approximated as follows

$$\text{6c.}\quad \rho(\bar{U}\bar{V})_{\mathrm{d}} = -\sqrt{\frac{f}{8}}\,\frac{\rho}{kH}\,U_{\mathrm{d}}V_{\max}\left(\frac{\pi^2 H}{18} - H\right)$$

The transverse velocity component $(\bar{V})$ is closely associated with the value of depth-averaged longitudinal velocity (U_{d}) in complex flow behaviour of a compound section (Ervine *et al*., 2000). So, $V_{\max}$ can be assumed to be a function of U_{d}. The value of the lateral gradient of the secondary flow $\rho(\bar{U}\bar{V})_{\mathrm{d}}$ is maximal in the mixing layer region because it scales with the lateral gradient of squared velocity (U_{d}^2). For a straight compound channel with rectangular main channel, the transverse

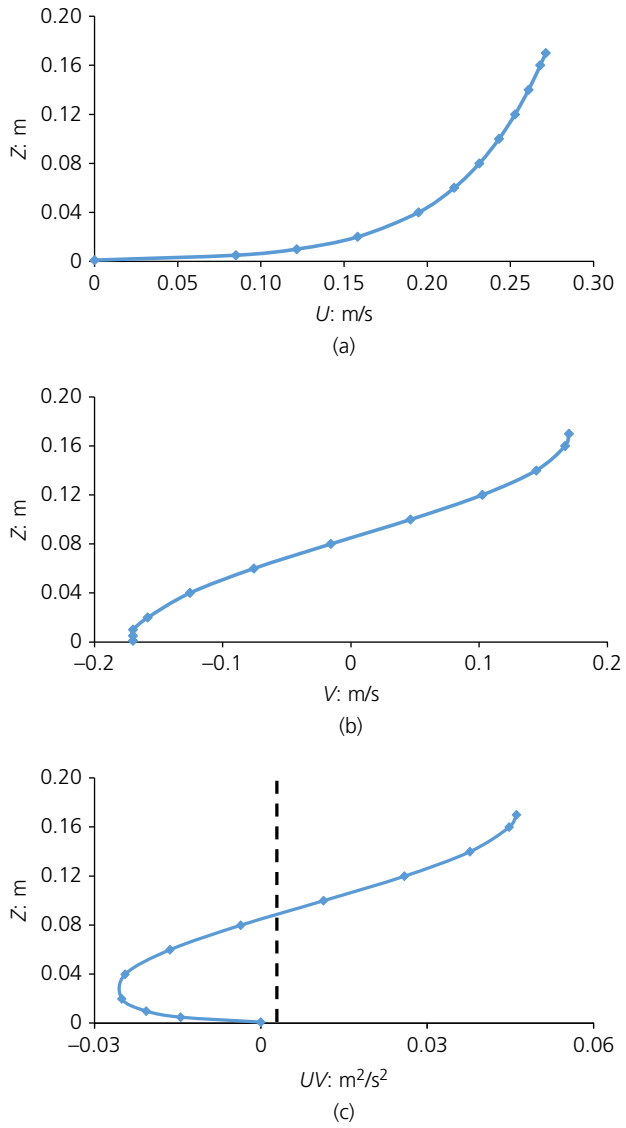

Figure 2. Vertical distribution of streamwise velocity, transverse velocity components and the product $\bar{U}\bar{V}$ (Van Prooijen *et al.* 2005)

velocity component $(\bar{V})$ varies within the range of 1–2% of longitudinal velocity $\bar{U}$ and it is in the range of 2–4% of longitudinal velocity in the trapezoidal main channel (Lorena, 1992).

For high Reynolds numbers in turbulent open channel flow, the turbulent shear stress $(-\rho\overline{u'v'})$ has been modelled by the eddy viscosity concept of the Boussinesq approach. The turbulent shear stresses due to bottom friction, together with the turbulent shear stress generated by the horizontal coherent structure are contributing to the momentum exchange. The turbulent shear stress (τ_{yx}) is expressed as

$$\text{6d.} \quad \tau_{yx} = \rho(\vartheta_{t1} + \vartheta_{t2})\frac{\partial U_\mathrm{d}}{\partial y}$$

ϑ_{t1} and ϑ_{t2} are the eddy viscosities due to bottom friction and large horizontal coherent structure, respectively. Proper estimations of these eddy viscosities are prerequisite to determine the accurate quantity of the Reynolds stresses. Both the contributions are quantified as the product of velocity and length scale to satisfy the dimension of kinematic eddy viscosity. The eddy viscosity characterising the bottom friction is modelled as per what has been done by previous researchers. Here, the flow depth (H) is taken as the length scale and shear velocity (U_*) is taken as the velocity scale. The contribution of the horizontal coherent structure to turbulent shear stress is caused by intense mixing at the junction and can be modelled according to Prandtl's mixing length theory. To achieve this, the mixing layer width (δ) is taken as the horizontal length scale and depth-averaged velocity (U_d) is taken as the velocity scale. The resultant Reynolds stress is now expressed as follows:

$$\text{6e.} \quad \tau_{yx} = \rho\lambda_1\sqrt{\frac{f}{8}}HU_\mathrm{d}\frac{\partial U_\mathrm{d}}{\partial y} + \rho l^2\left(\frac{\partial U_\mathrm{d}}{\partial y}\right)^2 = \rho\left(\lambda_1\sqrt{\frac{f}{8}}HU_\mathrm{d}\frac{\partial U_\mathrm{d}}{\partial y} + \lambda_2\delta U_\mathrm{d}\frac{\partial U_\mathrm{d}}{\partial y}\right)$$

λ_1 and λ_2 are the proportionality eddy viscosity constants for vertical and horizontal length scales. The significance of λ_1 and λ_2 is discussed later. The width of the mixing layer (δ) is decided by the mean velocities of the sub-sections (Van Prooijen *et al.*, 2005); this has been further quantified and found to be a function of flow depth (Devi and Khatua, 2016). Following this, the length of the mixing layer (δ) is expressed in terms of flow depth (H), as described in Devi and Khatua (2016) and Devi *et al.* (2016).

$$\text{6f.} \quad \delta = \left\{0.847\mathrm{e}^{2.371\left[1-(U_\mathrm{fp}/U_\mathrm{mc})\right]}\right\}H = C_\mathrm{m}H$$

where C_m is the non-dimensional coefficient of the mixing layer equal to $0.847\mathrm{e}^{2.371[1-(U_\mathrm{fp}/U_\mathrm{mc})]}$. U_mc and U_fp are defined as the respective depth-averaged mean velocities in the main channel and in the flood plain regions outside the mixing layer. Improvement of C_m has been achieved by taking more data sets of compound channels of different geometry and flow depths, which are discussed in the next section. So τ_{yx} is now reduced to

$$\text{6g.} \quad \tau_{yx} = \rho\left(\lambda_1\sqrt{\frac{f}{8}}HU_\mathrm{d}\frac{\partial U_\mathrm{d}}{\partial y} + \lambda_2 C_\mathrm{m}HU_\mathrm{d}\frac{\partial U_\mathrm{d}}{\partial y}\right)$$

The present objective is to predict both the depth-averaged velocity and the boundary shear stress for straight compound channel flow. The solutions to Equation 2 by previous investigators provide a good prediction of depth-averaged velocity

distribution but fail to predict the boundary shear distribution precisely. In many cases, neither of the variables is properly predicted, especially in the mixing layer region. This shortfall can be compensated by the use of a secondary flow contribution, Equation 6c, and a Reynolds stress contribution, Equation 6g. Using the two contributions, the new second-order linear differential equation becomes

$$\rho g H S_0 - \frac{f}{8}\rho U_d^2 + \frac{\partial}{\partial y} H \rho \left(\lambda_1 \sqrt{\frac{f}{8}} H U_d \frac{\partial U_d}{\partial y} + \lambda_2 C_m H U_d \frac{\partial U_d}{\partial y} \right) = \frac{\partial}{\partial y} H \left[-\sqrt{\frac{f}{8}} \frac{\rho}{kH} U_d V_{max} \left(\frac{\pi^2 H}{18} - H \right) \right] \quad (7a)$$

As described earlier and also found in Shiono and Knight (1991) and Van Prooijen *et al.* (2005), the value of $\bar{V}$ mostly lies in the range of 2–4% of $\bar{U}$ in the shear regions of FCF channels. So in the present study, the V_{max} value can be assumed as 4% of depth-averaged velocity (U_d). So, Equation 7a is simplified as

$$\rho g H S_0 - \frac{f}{8}\rho U_d^2 + \frac{\partial}{\partial y} H \rho \left(\lambda_1 \sqrt{\frac{f}{8}} H U_d \frac{\partial U_d}{\partial y} + \lambda_2 C_m H U_d \frac{\partial U_d}{\partial y} \right) = \frac{\partial}{\partial y} H \left[-\sqrt{\frac{f}{8}} \frac{\rho}{25kH} U_d^2 \left(\frac{\pi^2 H}{18} - H \right) \right] \quad (7b)$$

A sub-section of a compound channel may be considered as a constant flow depth domain or variable flow depth domain. Figure 3 shows the constant flow depth domain and linear side slope domain of a compound channel. Over the main channel bed and flood plain bed, the depth of flow is constant. However, over the side slope of the main channel, the depth of flow varies with lateral distance. The analytical solution to Equation 7b is now given as

$$U_d = \left[C_1 e^{\left((-B+\sqrt{B^2+4AC})/2A\right)y} + C_2 e^{\left((-B-\sqrt{B^2+4AC})/2A\right)y} + \frac{D}{C} \right]^{1/2} \quad (8a)$$

where $A = \rho\lambda_1 H^2/2\sqrt{f/8} + \rho\lambda_2 C_m H^2/2$

$$B = \frac{1}{25}\frac{\rho}{k}\sqrt{\frac{f}{8}}\left(\frac{\pi^2 H}{18} - H\right)$$

$$C = \rho\frac{f}{8}$$

$$D = \rho g S_0 H$$

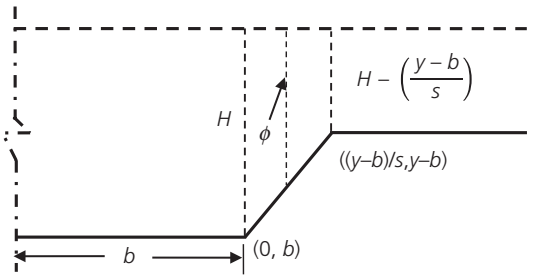

Figure 3. Constant flow depth domain and linear side slope domain

By applying proper boundary conditions, the unknown coefficients C_1 and C_2 for different flow zones can be obtained. The boundary conditions applied here are

- $U_{di} = U_{di+1}$ continuity of depth-averaged velocity
- $(dU_d/dy)_i = (dU_d/dy)_{i+1}$ continuity of lateral gradient of the depth-averaged velocity
- the velocity must be zero at the rigid sidewall (no-slip condition) of the flood plain $U_i = 0$
- $(dU_d/dy) = 0$ at the middle of the main channel (exclusively for symmetrical compound channel).

Using the relationship of depth-averaged velocity to boundary shear stress $\tau_b = f/8\rho U_d^2$, the expression for τ_b is written as

$$\tau_b = \rho\frac{f}{8}\left(C_1 e^{\left[(-B)+\sqrt{B^2+4AC}\right)/2A]y} + C_2 e^{\left[(-B)-\sqrt{B^2+4AC}\right)/2A]y} + \frac{D}{C} \right) \quad (8b)$$

In the case of no secondary currents, the term B becomes zero and the expressions of depth-averaged velocity and boundary shear stress are presented as

$$U_d = \left(C_1 e^{\sqrt{C/A}y} + A_2 e^{-\sqrt{C/A}y} + \frac{D}{C} \right)^{1/2}$$
$$\tau_b = \rho\frac{f}{8}\left(C_2 e^{\sqrt{C/A}y} + A_2 e^{-\sqrt{C/A}y} + \frac{D}{C} \right) \quad (8c)$$

Equations 8a–8c are not valid for the linear side slope domains as the depth of flow (H) in this region is a function of lateral dimension – that is, y. The varying depth of flow (ϕ) in linear side slope regions is expressed as

$$\phi = H - \left(\frac{y-b}{s}\right) \quad (9)$$

where H is the main channel flow depth; b is the semi-width of the main channel; and s is the main channel bank slope. Equation 7b is now reduced to the following form

$$\rho g\phi S_0 - \left[\frac{f}{8}\rho\left(1+\frac{1}{s^2}\right)^{1/2} + \sqrt{\frac{f}{8}}\frac{\rho}{25ks}\left(\frac{\pi^2}{18}-1\right)\right]U_d^2 + \left[\frac{\rho\lambda_1}{s^2}\sqrt{\frac{f}{8}} + \frac{\rho\lambda_2 C_m}{s^2} - \sqrt{\frac{f}{8}}\frac{\rho}{25ks}\left(\frac{\pi^2}{18}-1\right)\right]\phi\frac{\partial U_d^2}{\partial\phi} + \left(\frac{\rho\lambda_1}{2s^2}\sqrt{\frac{f}{8}} + \frac{\rho\lambda_2 C_m}{2s^2}\right)\phi^2\frac{\partial^2 U_d^2}{\partial\phi^2} = 0 \quad (10)$$

Equation 10 represents Cauchy's homogeneous linear equation. Such an equation is reduced to linear differential equations with constant coefficients. The analytical solution of this equation is given by

$$U_d = \sqrt{C_3\phi^{\frac{(L-M)+\sqrt{L^2+M^2-2L(M+2N)}}{2L}} + C_4\phi^{\frac{(L-M)-\sqrt{L^2+M^2-2L(M+2N)}}{2L}} - \frac{O}{M+N}\phi} \quad (11a)$$

where $L = \rho\lambda_1/2s^2\sqrt{f/8} + \rho\lambda_2 C_m/2s^2$

$$M = \frac{\rho\lambda_1}{s^2}\sqrt{\frac{f}{8}} + \frac{\rho\lambda_2 C_m}{s^2} - \sqrt{\frac{f}{8}}\frac{\rho}{25ks}\left(\frac{\pi^2}{18}-1\right)$$

$$N = -\left[\frac{f}{8}\rho\left(1+\frac{1}{s^2}\right)^{1/2} + \sqrt{\frac{f}{8}}\frac{\rho}{25ks}\left(\frac{\pi^2}{18}-1\right)\right]$$

$$O = \rho g S_0$$

The expression of boundary shear stress can be represented by

$$\tau_b = \rho\frac{f}{8}\left(C_3\phi^{\frac{(L-M)+\sqrt{L^2+M^2-2L(M+2N)}}{2L}} + C_4\phi^{\frac{(L-M)-\sqrt{L^2+M^2-2L(M+2N)}}{2L}} - \frac{O}{M+N}\phi\right) \quad (11b)$$

In the case of negligible secondary currents, the depth-averaged velocity and boundary shear stress can be evaluated by neglecting the second part of the terms M and N. By applying the above-mentioned boundary conditions, the unknown coefficients C_1, C_2, C_3 and C_4 for different flow zones can be obtained.

4. Application of the analytical model

The present analytical solution can be applied to a number of compound channels. For the solution of these Equations 7b and 10, the proper estimation of flow variables such as mixing layer coefficients C_m, friction factors of the sub-sections – that is, f_{mc} and f_{fp}, eddy viscosity coefficients – that is, λ_1 and λ_2 are to be determined.

4.1 Estimation of mixing layer coefficient, C_m

Both Equations 7b and 10 contain the coefficient of mixing layer (C_m), which can be estimated using Equation 6f. For more practical application, Equation 6f is further refined by taking a large number of data sets of compound channels. From the definition of shear layer width (δ) as given by Van Prooijen *et al.* (2005), the values of δ have been estimated for channels with different geometries and flow depths (Table 1). The ranges of width ratio (α) and relative flow depths (β) considered are from 2 to 12 and from 0.05 to 0.5, respectively. The width ratio (α) is defined as the ratio of total width of the compound channel to the bottom width of the main channel and relative flow depth (β) is defined as the ratio of flow depth over the floodplain to that of the main channel.

Non-dimensional mixing layer width (δ/H) against the mean velocity ratio of the sub-sections ($(U_{mc} - U_{fp})/U_{mc}$) is plotted in Figure 4 for all the channels. The best fit between these two variables has been chosen as an exponential function with a regression coefficient of 0.80 as

$$\delta = \left(0.733e^{2.115\left(1-U_{fp}/U_{mc}\right)}\right)H = C_m H \quad (12)$$

The magnitude of the mean velocity ratios between the flood plain and main channel (U_{fp}/U_{mc}) can be simplified from a proper flow distribution expression. Knight and Demetriou (1983), Khatua and Patra (2009), Mohanty and Khatua (2014) and Devi *et al.* (2016) expressed the percentage of flow in the sub-sections of compound channels for different ranges of width ratio. Devi *et al.* (2016) derived a generalised equation for estimating the percentage of flow in the main channel (% Q_{mc}) valid for a large range of width ratio from 2 to 12, which is demonstrated as

$$\%Q_{mc} = 1.715\%A_{mc}^{0.9} \quad (13)$$

Table 1. Details of geometric and roughness parameters of large-scale FCF and small-scale flumes

Test channel	Cross-sectional geometry	Total width, B: m	Main channel width, b_2: m	Differential roughness, γ	Bank slope (V:H)	Mannings n, n_{mc} and n_{fp}	Main channel depth, h: m	Longitudinal slope, S_0	Width ratio, α	Aspect ratio, δ
FCF-series 1	Trapezoidal	10.005	1.5	1	01 : 01	0.01	0.15	0.001027	6.67	10
FCF-series 2	Trapezoidal	6.3	1.5	1	01 : 01	0.01	0.15	0.001027	4.2	10
FCF-series 3	Trapezoidal	3.3	1.5	1	01 : 01	0.01	0.15	0.001027	2.2	10
FCF-series 6	Trapezoidal	4.05	1.5	1	01 : 01	0.01	0.15	0.001027	2.7	10
FCF-series 8	Rectangular	6	1.5	1	—	0.01	0.15	0.001027	4	10
FCF-series 10	Trapezoidal	6.6	1.5	1	01 : 02	0.01	0.15	0.001027	4.4	10
NITR-series 1	Trapezoidal	1.68	0.33	1	01 : 01	0.01	0.11	0.001	5.1	3
NITR-series 2	Trapezoidal	1.45	0.33	1	01 : 01	0.01	0.11	0.001	4.4	3
NITR-series 3	Trapezoidal	1.19	0.33	1	01 : 01	0.01	0.11	0.001	3.6	3
Rezaei (2006) S1	Rectangular	0.60	0.4	1	—	0.0088	0.05	0.002003	1.5	8
Rezaei (2006) S2	Rectangular	0.80	0.4	1	—	0.0088	0.05	0.002003	2	8
Rezaei (2006) S3	Rectangular	1.00	0.4	1	—	0.0088	0.05	0.002003	2.5	8
Rezaei (2006) S4	Rectangular	1.20	0.4	1	—	0.0088	0.05	0.002003	3	8
Yuen (1989)	Trapezoidal	0.45	0.15	1	01 : 01	0.0092	0.075	0.001	3	2
Atabay (2001) S1	Rectangular	1.21	0.398	1	—	0.0091	0.05	0.002024	3.04	7.96
Atabay (2001) S2	Rectangular	0.8053	0.398	1	—	0.0091	0.05	0.002024	2.02	7.96

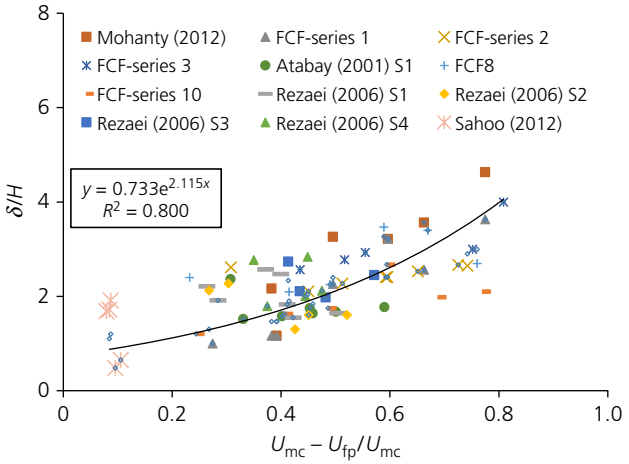

Figure 4. Variation of non-dimensional mixing layer width (δ/H) with the mean velocity ratio of the sub-sections ($(U_{mc} - U_{fp})/U_{mc}$)

Utilising the above expression of $\%Q_{mc}$, the mean velocity ratio between the flood plain and main channel (U_{fp}/U_{mc}) is simplified as

$$14. \quad \frac{U_{fp}}{U_{mc}} = \frac{0.924 \times A^{0.9} A_{mc}^{0.1} - A_{mc}}{A_{fp}}$$

where A_{mc}, A_{fp} and A are the flow area of the main channel, flood plain and total compound channel, respectively. Now Equations 12 and 14 are utilised to estimate the coefficient of mixing layer width C_m of a compound channel.

4.2 Selection of zonal friction factor

Darcy–Weisbach friction factors for the main channel (f_{mc}) and flood plain (f_{fp}) sub-sections can be obtained from a relationship depending upon the hydraulic depth of sub-sections and bottom roughness values in terms of Manning's n, as given below (Fernandes *et al.*, 2014).

$$15. \quad f_{mc} = \frac{8gn_{mc}^2}{R_{mc}^{1/3}} \text{ and } f_{fp} = \frac{8gn_{fp}^2}{R_{fp}^{1/3}}$$

where n_{mc}, n_{fp} and R_{mc}, R_{fp} are the respective Manning's n and hydraulic depth values for the sub-sections.

4.3 Consideration of eddy viscosity coefficients λ_1 and λ_2

The eddy viscosity coefficients λ_1 and λ_2 in the proposed analytical model characterise the intensity of the Reynolds shear stress during overbank flow events. Effective total eddy viscosity due to the bottom turbulence (λ_1) and horizontal

coherent structures (λ_2) for both higher flow depth and lower flow depth cases ($\beta = 0.11$ and $\beta = 0.25$) were plotted by Knight and Shiono (1990). Similarly, individual variations of eddy viscosity due to bottom turbulence and horizontal coherent structures for both higher and lower flow depths were presented by Van Prooijen *et al*. (2005). It is noticed from their results that there is much variation of eddy viscosity due to the horizontal coherent structures along the channel perimeter as compared to bottom turbulence. This confirms the estimation of proportionality coefficients of eddy viscosities – that is, λ_1 and λ_2. These values are calibrated using a large number of experimental data sets from previous investigators and rivers, as given in Tables 1 and 2.

While applying the present solutions to fit the observed depth-averaged velocity and boundary shear stress distribution values, the calibrating parameter λ_1 is found to be insensitive to the solution, confirming the findings from Knight and Abril (1996). However, the model is found to be sensitive to λ_2 values. The values of λ_2 are found to vary from zone to zone of both FCF channels and compound river sections. A small deviation of this value produces a large deviation in boundary shear stress and depth-averaged velocity results. In the initial test runs, the values of λ_1 and λ_2 are estimated and successfully refined until they give best fits with the observed lateral depth-averaged velocity and boundary shear stress distribution data. Here, the magnitude of coefficient of eddy viscosity due to the bottom friction (λ_1) is adopted according to Knight and Abril (1996). The eddy viscosity coefficient for the main channel (λ_{1mc}) has been taken as 0.067 and, for the flood plain (λ_{1fp}), it is adopted as suggested by Abril and Knight (2004) and Knight (2007). The relationship is expressed as

$$16. \quad \lambda_{1fp} = \lambda_{1mc}\left(-0.2 + 1.2\beta^{-1.44}\right)$$

The dimensionless eddy viscosity coefficient λ_2 characterises the momentum exchange intensity due to the horizontal coherent structure (Van Prooijen *et al*., 2005). Interestingly, for a particular value of λ_2, it can be seen that in the floodplain region both the transverse velocity and boundary shear stress distribution provide better results. But, in the main channel region these values vary from flow depth to flow depth and from channel to channel. Accounting for these values also provides good results in the shear layer regions of all channels, which confirms that both the bottom turbulence and horizontal coherent structure play important roles for flow modelling in both the shear layer region and outside the shear layer region. This justifies the need for individual eddy viscosity coefficients due to a horizontal coherent structure for the main channel (λ_{2mc}) and for the flood plain (λ_{2fp}).

Studying the variation of λ_{2mc} for a number of channels – for example, FCF, Rezaei (2006), Yuen (1989), Atabay (2001) and natural rivers – the dependency of λ_{2mc} on the width ratio, relative flow depth and friction factor ratio are analysed. From Figure 5(a), it can be seen that the values of λ_{2mc} follow a rising trend with width ratio while there is a falling trend with relative flow depth, as shown in Figure 5(b). To analyse the effect of roughness on the eddy viscosity coefficients (λ_{2mc}), the friction factor ratio is taken into consideration, which is defined as the ratio between the flood plain friction factor (f_{fp}) and the main channel friction factor (f_{mc}). From the dependency shown in Figure 5(c), a falling trend is revealed for λ_{2mc} with friction factor ratio (f_{fp}/f_{mc}). It can therefore be clearly shown that λ_{2mc} is influenced by these three non-dimensional parameters (α, β and f_{fp}/f_{mc}). Analysing the dependencies from Figures 5(a)–5(c) and compiling the effects of α, β and f_{fp}/f_{mc}, the final expression of the eddy viscosity coefficient characterising the horizontal coherent structure for the main channel zone is expressed as

$$17. \quad \lambda_{2mc} = 0.0002\alpha^{1.514}\beta^{-1.49}\left(\frac{f_{fp}}{f_{mc}}\right)^{-0.965}$$

The λ_{2mc} values found from the fitting of the depth-averaged curve and boundary shear stress curves are compared with the predicted values using Equation 17 and the results are shown in Figure 6.

The additional coefficients for the side slope – namely, λ_{2s} – and for the flood plain regions – namely, λ_{2fp} – also need to be approximated for the present solution. These two values show little variation when fitted to all experimental data sets; therefore, unique values for individual sub-sections can be adopted for these parameters. The values of these coefficients are taken as 0.01 for the side slope region (λ_{2s}) and 0.001 for flood plain region (λ_{2fp}). Utilising these three values – that is, λ_{2fp}, λ_{2s} and

Table 2. Error values of the predictions from the present and existing models for experimental channels

Different model	MAE	MAPE	RMSE	R^2	E	I_d
Present approach	0.033	9.86	0.046	0.912	0.98337	0.998736
SKM	0.068	16.22	0.095	0.835	0.867559	0.918174
Knight *et al*. (2007)	0.042	11.43	0.072	0.886	0.97911	0.994909
Tang and Knight (2008)	0.058	12.25	0.089	0.865	0.974993	0.994187

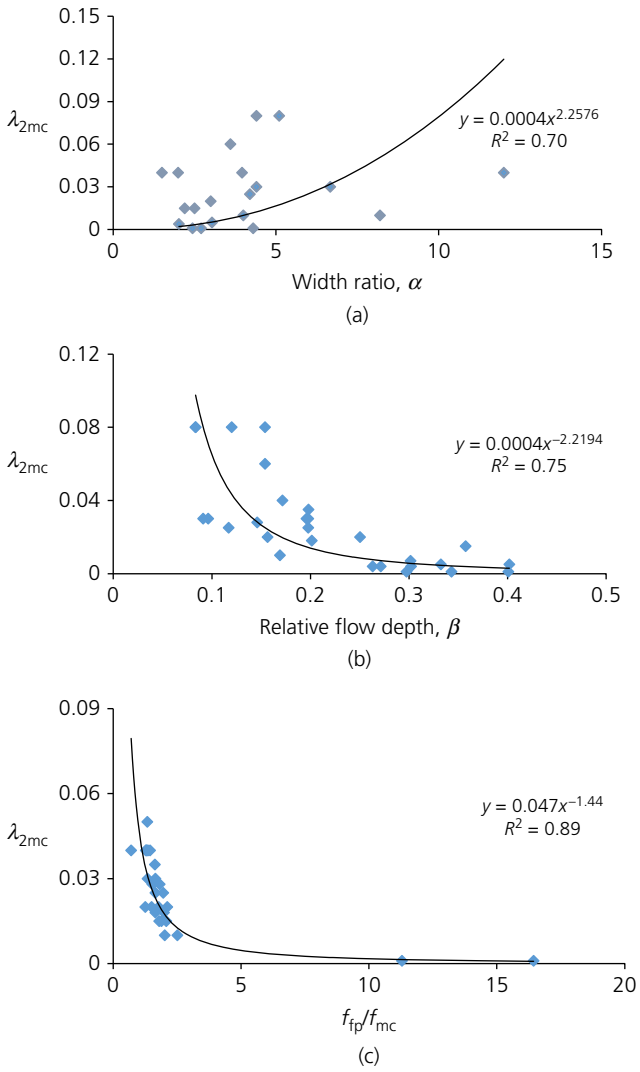

Figure 5. Dependency of λ_{2mc} on (a) width ratio (α), (b) relative flow depth (β) and (c) friction factor ratio (f_{fp}/f_{mc})

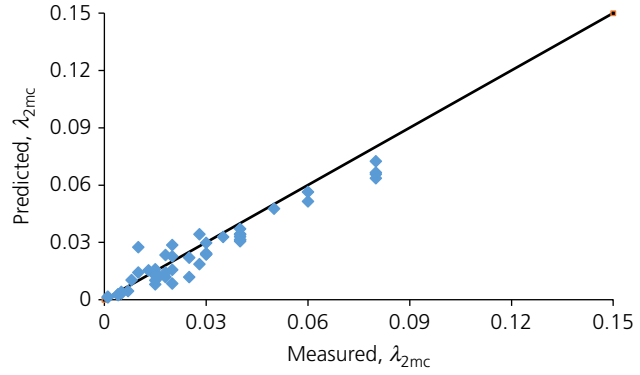

Figure 6. Comparison between predicted λ_{2mc} and measured λ_{2mc}

λ_{2mc} – the present solution produces precise results of flow variables for all the experimental channels, including the river geometries, which is described in the next section.

4.4 Estimation of depth-averaged velocity and boundary shear stress distribution in compound channel

The analytical model is first applied to estimate the depth-averaged velocity and boundary shear stress distribution of FCF straight channels for both symmetric and asymmetric flood plains. Then, experimental channels from previous investigations are utilised as well to examine the applicability of the model, as shown in Figure 7. The details of the geometrical and hydraulic parameters of all experimental channels considered for the present analysis are presented in Table 1.

5. Comparison with existing models

An attempt has been made to compare the present approach with well-known models of Shiono and Knight (1991), Knight *et al.* (2007) and Tang and Knight (2008). FCF-series 1, FCF-series 6 and NITR-series 1 are taken for the comparison. Figure 8 demonstrates the comparison of these model results along with the present approach with their experimental values.

Further, to demonstrate the significance of the approach, an error analysis is conducted for all of the estimated U_d values resulting from all models. This analysis is required for a deep understanding regarding the strength of the analytical model developed and to give an insight into the importance of all input parameters. Using Equation 18, the error analysis has been carried out for some depth-averaged velocity distributions by comparing the predictions from the new approach and from previous approaches, such as Shiono and Knight (1991), Knight *et al.* (2007) and Tang and Knight (2008). This step shows the variance of predicted values from the observed one for experimental channels. Six types of errors – mean absolute error (MAE), mean absolute percentage error (MAPE), root mean square error (RMSE), Nash–Sutcliffe efficiency (E), index of agreement (I_d) and coefficient of determination (R^2) – are considered to evaluate the performance of all models. The expressions for these six types of errors are computed as per the following equations (Das and Khatua, 2018):

$$\text{18a.} \quad \text{MAE} = \frac{1}{N}\sum|O_i - P_i|$$

$$\text{18b.} \quad \text{MAPE} = \frac{1}{N}\sum 100 \times \frac{|O_i - P_i|}{O_i}$$

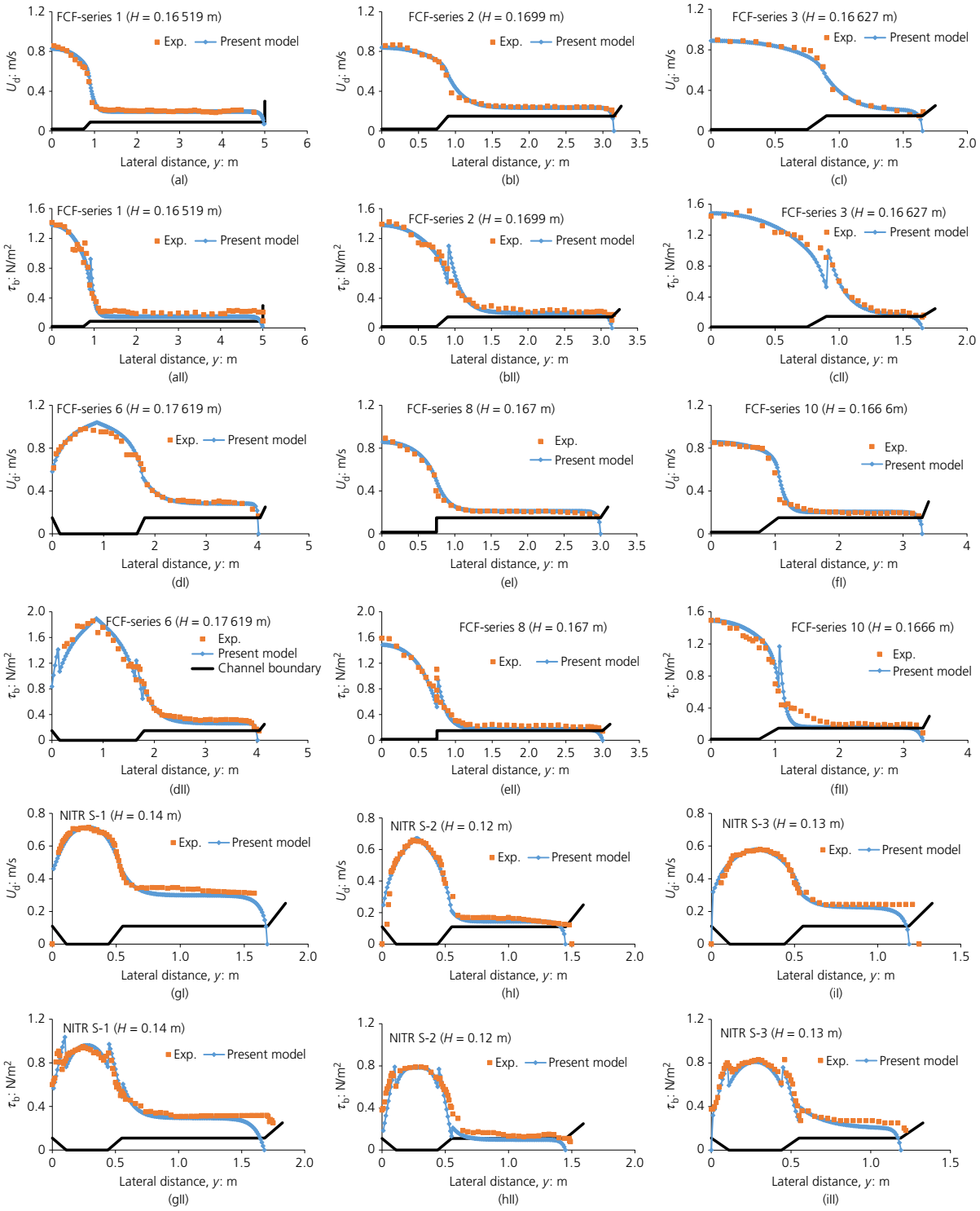

Figure 7. (a I)–(p II) Depth-averaged velocity and boundary shear stress distribution for different experimental channels (continued on next page)

18c. $$\mathrm{RMSE} = \sqrt{\frac{1}{N}\sum\left(\frac{O_i - P_i}{O_i}\right)^2}$$

18d. $$E = 1 - \frac{\sum (O_i - P_i)^2}{\sum (O_i - O_{i\,\mathrm{mean}})^2}$$

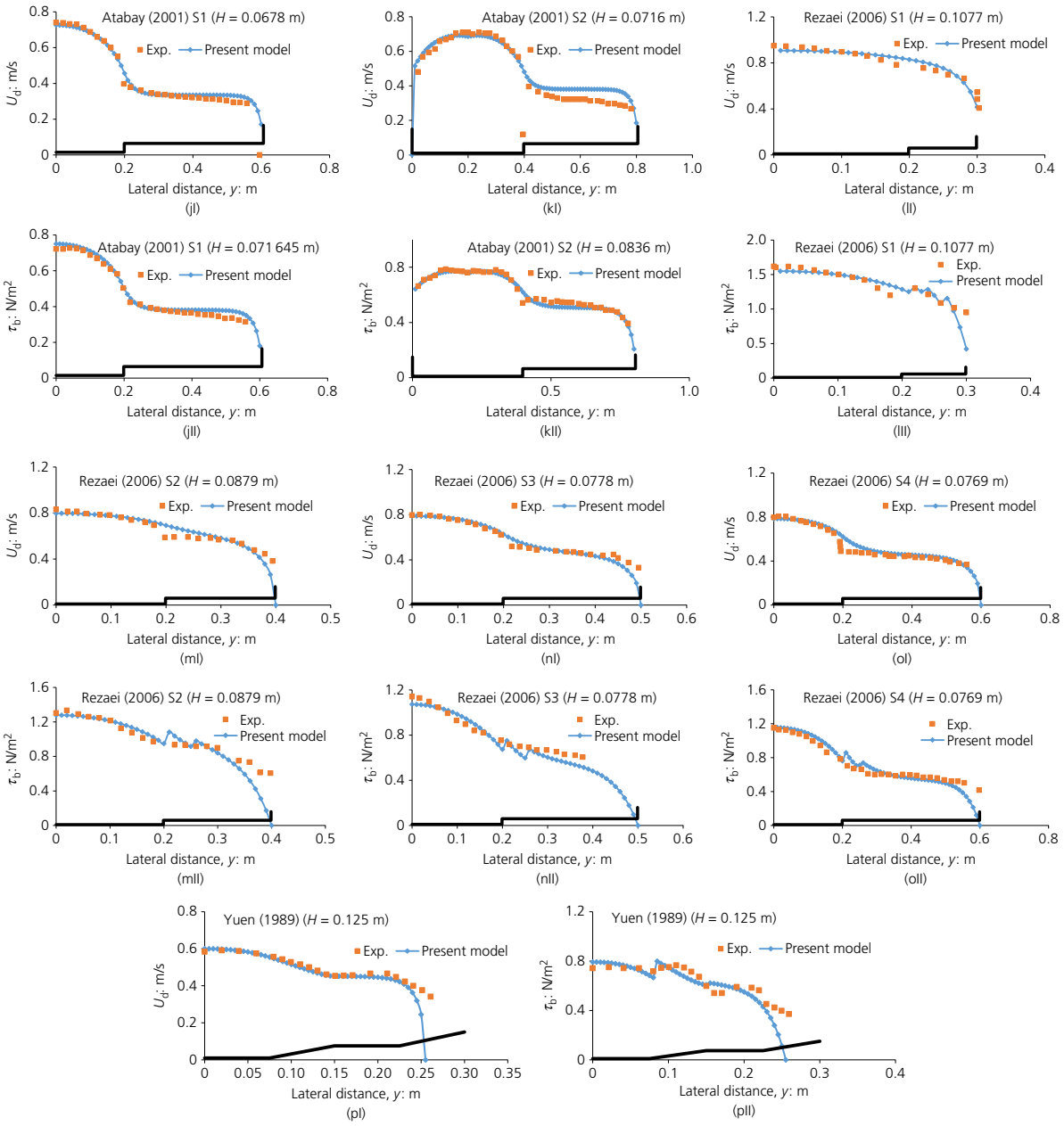

Figure 7. Continued

18e. $$I_d = 1 - \frac{\sum_i^N (O_i - P_i)^2}{\sum_i^N (|P_i - O_{i\,\text{mean}}| + |O_i - O_{i\,\text{mean}}|)^2}$$

18f. $$R^2 = \left\{ \frac{\sum O_i P_i - (\sum O_i)(\sum P_i)}{\sqrt{\left[N \sum O_i^2 - (\sum O_i)^2\right]\left[N \sum P_i^2 - (\sum P_i)^2\right]}} \right\}^2$$

where P_i denotes the predicted values; O_i denotes the observed values; $O_{i\ \text{mean}}$ is the mean of the observed values; and N is the number of samples. The error values are given in Table 2. It is found from Table 2 that the present method can predict the experimental flow variables with reasonable accuracy. This is because the present analytical model incorporates both the turbulent shear stress and secondary flow contribution of a compound open channel flow.

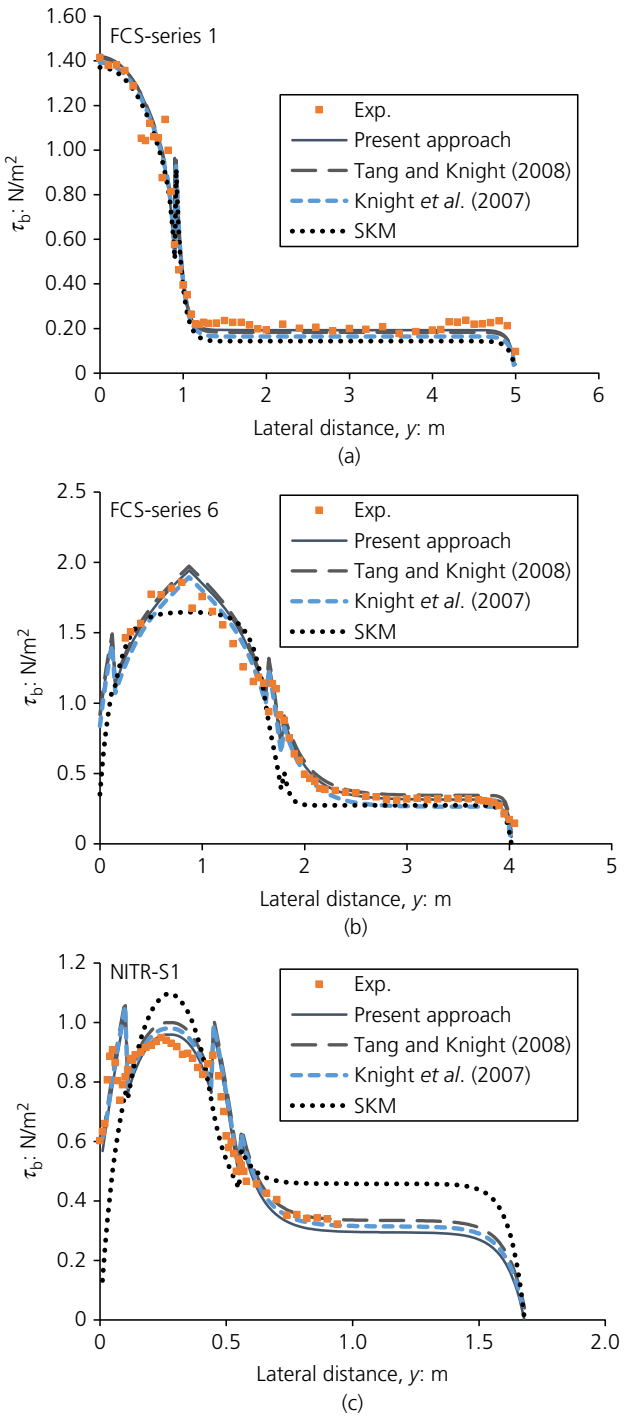

Figure 8. (a)–(c) Comparison of present approach with previous models for experimental channels

6. Practical application of the present model to river channels

The new model is also applied to tsix natural river channels with different cross-sectional geometry and roughness on their sub-section perimeters. These are the rivers Batu, Senggai, Senggi B, Severn, Trent and Main. The geometrical, hydraulic and surface conditions of the rivers are presented in Table 3. These data sets are extracted from McGahey *et al.* (2006) and Hin *et al.* (2008). Owing to the unavailability of the boundary shear stress data sets, only predicted depth-averaged velocity (U_d) results across the river channels are presented and the comparisons of these with the observed values are shown in Figure 8.

One more interesting and promising feature has also been observed, in that the present expression of secondary flow term depends on the value of the highest lateral velocity component V_{max}, which is generally 2–4% of the depth-averaged velocity (U_d). This has been confirmed by many investigators, including Lorena (1992) and Ervine *et al.* (2000). This value has therefore been incorporated for estimating the results of depth-averaged velocity (U_d) and boundary shear stress (τ_b) distribution of all the compound channels, except FCF-series 2 ($\alpha = 4.2$) and series 3 ($\alpha = 2.2$). Good predictions of U_d and τ_b are found in the main channel and flood plain regions of these lower width ratio channels, except at the shear layer regions of flood plains. A sudden drop in the predicted values is noticed near the junctions of the shear layer region, which may be due to inclusion of improper secondary flow contributions and enormous turbulence. According to the results of depth-averaged velocity and secondary flow vectors (for FCF-series 2) shown in Shiono and Knight (1991), it is confirmed that a higher magnitude of lateral maximum velocity component V_{max} occurs in the shear layer region of the flood plains. The order of these magnitudes is found to be about 20% of the longitudinal velocity (U_d) of the shear layer region. By taking this amount of V_{max} values in the secondary flow term of Equation 6c, a substantial improvement to the depth-averaged velocity and boundary shear stress distribution are noticed at both the shear layer region and outside the shear layer regions. So, for FCF-series 2 and FCF-series 3, the boundary shear stress predictions are improved in the interface regions by adopting a greater value of V_{max} for the large-scale secondary flow generated in the shear layer region.

The results demonstrated in Figures 7 and 9 present good predictions of flow variables for experimental channels and natural rivers. Table 4 indicates the error analysis of the present model for the different river channels. It is found that for river channels, the present model provides an error in depth-averaged velocity calculation in terms of MAE, MAPE and RMSE values of less than 0.12, 20% and 0.35, respectively, and also provides a high R^2 value in the range of 0.85–0.91.

7. Conclusions

An analytical solution to the depth-integrated turbulent form of the Navier–Stokes equation is presented. The transverse shear stress in the mixing region is modelled using an effective eddy

Table 3. Geometrical and flow parameters of the river data sets

Natural river	Max. width, B: m	Bank full width, b_2: m	Bank full depth, h: m	Longitudinal slope, S_0		Width ratio, α	Flow depth, H: m	Surface condition	
				Main channel	Flood plain			Main channel (n_{mc})	Flood plain (n_{fp})
Batu (Kuching)	78	5.15	1.55	0.0016	0.0013	4.3	2.243	Large boulder (0.062)	Long vegetation (0.25)
Senggai (Kuching)	76	6.75	1.06	0.001	0.001	40	1.587	Erodible soil (0.025)	Long vegetation (0.035)
Senggi B (Kuching)	25	5.50	1.30	0.001	0.00085	12	2.13	Erodible soil (0.082)	Long vegetation (0.25)
Severn (Montford Bridge)	135	35	5.75	0.000195	0.000195	8.2	6.92	Grass (0.032)	Grass covered (0.04)
Trent (Yoxall)	80	37.5	2.1	0.001	0.001	3.96	2.535	Gravel (0.032)	Grass and bushes (0.015)
Main (County Antrim)	38	13.60	0.90	0.003	0.003	2.44	1.37	Coarse gravel (0.032)	Short vegetation (0.09)

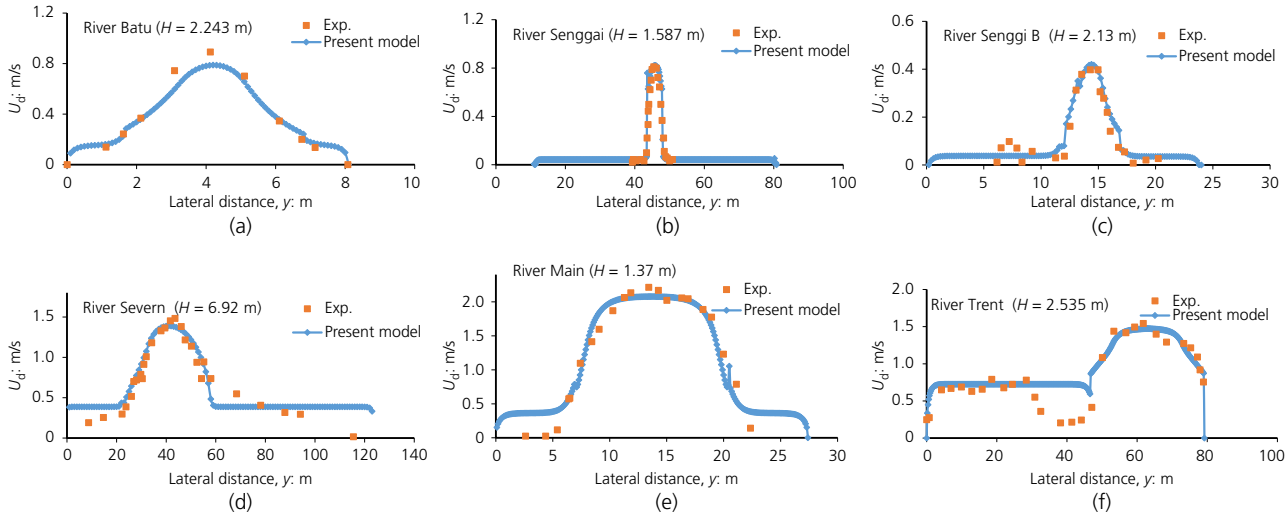

Figure 9. (a)–(f) Depth-averaged velocity distribution for rivers

Table 4. Error values of the predictions from the present model for different river channels

River channels	MAE	MAPE	RMSE	R^2	E	I_d
River Batu	0.056	12.62	0.136	0.876	0.936	0.886
River Senggi	0.064	14.63	0.106	0.894	0.925	0.864
River Senggi B	0.086	13.52	0.089	0.912	0.907	0.865
River Severn	0.172	19.56	0.286	0.855	0.922	0.854
River Main	0.106	17.21	0.325	0.864	0.95	0.879
River Trent	0.113	16.78	0.266	0.889	0.903	0.836

viscosity concept that contains horizontal coherent structures and three-dimensional bottom turbulence. A mathematical expression to estimate the value of the eddy viscosity coefficient for the main channel characterising the horizontal coherent structure is developed for channels of different geometry, flow and roughness conditions. The secondary flow term in the SKM is also modelled to improve the results for flow variables, especially in the shear layer region. An analytical solution is successfully applied to a number of compound channels of different geometry and flow conditions. The present model provides better results with minimum error as compared to other existing models, such as SKM and the models of Knight *et al.* (2007) and Tang and Knight (2008), in predicting the depth-averaged velocity and boundary shear stress in the main channel, flood plain and side slope of compound channels. The efficacy of the present model is also tested with natural rivers and found to be successful in predicting depth-averaged velocity under different geometry and flow conditions.

Acknowledgement

Previous researchers are acknowledged in particular for their experimental data sets and the researchers listed in the References section are appreciated for their key findings. The data used are listed in tables such that readers can find and access these data.

REFERENCES

Abril JB and Knight DW (2004) Stage-discharge prediction for rivers in flood applying a depth-averaged model. *Journal of Hydraulic Research* **42(6)**: 616–629.

Atabay S (2001) *Stage-discharge, Resistance and Sediment Transport Relationships for Flow in Straight Compound Channels*. Doctoral dissertation, University of Birmingham, Birmingham, UK.

Das BS and Khatua KK (2018) Flow resistance in a compound channel with diverging and converging floodplains. *Journal of Hydraulic Engineering* **144(8)**: 04018051.

Devi K and Khatua KK (2016) Prediction of depth averaged velocity and boundary shear distribution of a compound channel based on the mixing layer theory. *Flow Measurement and Instrumentation* **50**: 147–157.

Devi K, Khatua KK and Khuntia JR (2016) Prediction of mixing layer in symmetric and asymmetric compound channels. In *River Flow 2016* (Constantinescu G, Garcia M and Hanes D (eds)). CRC Press, Leiden, the Netherlands, pp. 39–47.

Ervine DA, Babaeyan-Koopaei K and Sellin RH (2000) Two-dimensional solution for straight and meandering overbank flows. *Journal of Hydraulic Engineering* **126(9)**: 653–669.

Fernandes JN, Leal JB and Cardoso AH (2014) Improvement of the lateral distribution method based on the mixing layer theory. *Advances in Water Resources* **69**: 159–167.

Hin LS, Bessaih N, Ling LP *et al.* (2008) Discharge estimation for equatorial natural rivers with overbank flow. *International Journal of River Basin Management* **6(1)**: 13–21.

Kawahara Y and Tamai N (1988) Note on turbulence modeling for secondary flows in passages of non-circular cross-section. *Doboku Gakkai Ronbunshu* **1988(399)**: 247–250.

Khatua KK and Patra KC (2007) Boundary shear stress distribution in compound open channel flow. *ISH Journal of Hydraulic Engineering* **13(3)**: 39–54.

Khatua KK and Patra KC (2009) Flow distribution in meandering compound channel. *ISH Journal of Hydraulic Engineering* **15(3)**: 11–26.

Knight DW (2007) Modelling overbank flows in rivers – data, concepts, models and calibration. In *Numerical Modelling of Hydrodynamics for Water Resources: Proceedings of the Conference on Numerical Modelling of Hydrodynamic Systems, Zaragoza, Spain* (Navarro PC and Playan E (eds)). Taylor & Francis/Balkema, Leiden, the Netherlands, pp. 3–23.

Knight DW and Abril CJB (1996) Refined calibration of a depth-averaged model for turbulent flow in a compound channel. *Proceedings of the Institution of Civil Engineers. Water, Maritime and Energy* **118(3)**: 151–159, https://doi.org/10.1680/iwtme.1996.28682.

Knight DW and Demetriou JD (1983) Flood plain and main channel flow interaction. *Journal of Hydraulic Engineering* **109(8)**: 1073–1092.

Knight DW and Shiono K (1990) Turbulence measurements in a shear layer region of a compound channel. *Journal of Hydraulic Research* **28(2)**: 175–196.

Knight DW, Omran M and Tang X (2007) Modeling depth-averaged velocity and boundary shear in trapezoidal channels with secondary flows. *Journal of Hydraulic Engineering* **133(1)**: 39–47.

Kordi H, Amini R, Zahiri A and Kordi E (2015) Improved Shiono and Knight method for overflow modeling. *Journal of Hydrologic Engineering* **20(12)**: 04015041.

Krishnappan BG and Lau YL (1986) Turbulence modeling of flood plain flows. *Journal of Hydraulic Engineering* **112(4)**: 251–266.

Lambert MF and Sellin RHJ (1996) Discharge prediction in straight compound channels using the mixing length concept. *Journal of Hydraulic Research* **34(3)**: 381–394.

Larsson R (1986) Coriolis generated secondary currents in channels. *Journal of Hydraulic Engineering* **112(8)**: 750–767.

Lorena MLMDLDS (1992) *Meandering Compound Flow*. Doctoral dissertation, University of Glasgow, Glasgow, Scotland.

McGahey C, Samuels PG and Knight DW (2006) *A Practical Approach to Estimating the Flow Capacity of Rivers–Application and Analysis*. Taylor and Francis, London, UK, pp. 303–312.

Mohanty PK (2012). *Flow Analysis of Compound Channels with Wide Flood Plains*. Doctoral dissertation, National Institute of Technology, Rourkela, India.

Mohanty PK and Khatua KK (2014) Estimation of discharge and its distribution in compound channels. *Journal of Hydrodynamics, Series B* **26(1)**: 144–154.

Prinos P, Townsend R and Tavoularis S (1985) Structure of turbulence in compound channel flows. *Journal of Hydraulic Engineering* **111(9)**: 1246–1261.

Rameshwaran P and Shiono K (2007) Quasi two-dimensional model for straight overbank flows through emergent. *Journal of Hydraulic Research* **45(3)**: 302–315.

Rezaei B (2006) *Overbank Flow in Compound Channels with Prismatic and non-Prismatic Floodplains*. Doctoral dissertation, University of Birmingham, Birmingham, UK.

Sahoo N (2012) *Effect of Differential Roughness on Flow Characteristics in a Compound Open Channel*. MTech by Research dissertation, National Institute of Technology, Rourkela, India.

Shiono K and Knight DW (1989) Transverse and vertical Reynolds stress measurements in a shear layer region of a compound channel. In *Proceedings of the 7th Symposium on Turbulent Shear Flows, Stanford, UK*, vol. 28, pp. 1–6.

Shiono K and Knight DW (1991) Turbulent open-channel flows with variable depth across the channel. *Journal of Fluid Mechanics* **222**: 617–646.

Shiono K and Rameshwaran P (2015) Mathematical modelling of bed shear stress and depth averaged velocity for emergent vegetation on floodplain in compound channel. In *Proceedings of 36th IAHR World Congress, The Hague, The Netherlands*.

Tang X and Knight DW (2008) Lateral depth-averaged velocity distributions and bed shear in rectangular compound channels. *Journal of Hydraulic Engineering* **134(9)**: 1337–1342.

Tominaga A and Nezu I (1991) Turbulent structure in compound open-channel flows. *Journal of Hydraulic Engineering* **117(1)**: 21–41.

Tominaga A, Nezu I, Ezaki K and Nakagawa H (1989) Three-dimensional turbulent structure in straight open channel flows. *Journal of Hydraulic Research* **27(1)**: 149–173.

Uijttewaal WSJ and Booij R (2000) Effects of shallowness on the development of free-surface mixing layers. *Physics of Fluids* **12(2)**: 392–402.

Van Prooijen BC and Uijttewaal WS (2002) A linear approach for the evolution of coherent structures in shallow mixing layers. *Physics of Fluids* **14(12)**: 4105–4114.

Van Prooijen BC, Battjes JA and Uijttewaal WS (2005) Momentum exchange in straight uniform compound channel flow. *Journal of Hydraulic Engineering* **131(3)**: 175–183.

Wormleaton PR (1996) Floodplain secondary circulation as a mechanism for flow and shear stress redistribution in straight compound channels. In *Coherent Flow Structures in Open Channels* (Ashworth PJ, Bennett SJ, Best JL and McLelland SJ (eds)). John Wiley & Sons, Washington, DC, USA, pp. 581–608.

Yang SQ, Tan SK and Lim SY (2004) Velocity distribution and dip-phenomenon in smooth uniform open channel flows. *Journal of Hydraulic Engineering* **130(12)**: 1179–1186.

Yuen KWH (1989) *A Study of Boundary Shear Stress, Flow Resistance and Momentum Transfer in Open Channels with Simple and Compound Trapezoidal Cross Sections.* Doctoral dissertation, University of Birmingham, Birmingham, UK.